Pure Appl. Chem., Vol. 82, No. 1, pp. 321–337, 2010.
doi:10.1351/PAC-CON-08-12-08

Spectral element analysis of the blood flow in human arteries*

Usik Lee‡ and Injoon Jang

Department of Mechanical Engineering, 253 Yonghyun-Dong, Nam-Gu, Incheon 402-751, South Korea

Abstract: It has been well recognized that cardiovascular diseases are closely related to blood flow characteristics. Thus, how to predict them accurately enough in an efficient way has been an important research issue. This paper introduces a 1D spectral element model for the blood flow in the human arteries with varying cross-sections. The variational approach is used to formulate the 1D spectral element model. The exact wave solutions to the frequency-domain governing differential equations are used to determine the frequency-dependent shape functions. The spectral finite element model is then applied to some example arteries to investigate flow characteristics such as blood flow rate and blood pressure through the arteries.

Keywords: arteries; blood flow rate; blood pressure; blood vessels; spectral element method.

INTRODUCTION

It has been well recognized that blood flow characteristics determine the wall shear stress and wall tension which are closely related to cardiovascular diseases such as aneurysm and stenosis. Thus, it has become very important to predict blood flow characteristics accurately in an efficient way for cardiovascular disease research, surgical planning, or medical device design. To this end, during the last decade, the computational methods have merged as the powerful tools for the modeling and analysis of the blood flow rate and pressure in arteries.

Modeling of blood flow and pressure has been studied intensively during the last decade, and various computational models have been reported in the literature [1–10]. The computational models of blood flow can be classified into the lumped parameters models [1,2], the 1D wave propagation models [3–6], and the 3D models [7–10]. The 1D models have been widely used because it enables us to obtain clinically relevant information on local mean blood flow and pressure waves through arterial systems very efficiently as well as the boundary conditions suitable for 3D models. For solving 1D models of blood flow, the two-step Lax–Wendroff method [5] and finite element method (FEM) [6–10] have been applied. To the authors' best knowledge, however, the spectral element method (SEM) has not been applied to the modeling and analysis of the blood flow through human arteries.

The FEM is certainly one of most powerful computational methods for solving diverse complex engineering problems. To formulate the conventional finite element models, the simple polynomials that are not related to vibration frequency are used as the shape functions. Thus, one may need very fine meshing in order to improve the FEM solutions, especially at high frequency: this may increase the computation cost and time significantly. In contrast to the conventional FEM, the SEM is an exact so-

*Paper based on a presentation at the 13th International Biotechnology Symposium (IBS 2008): "Biotechnology for the Sustainability of Human Society", 12–17 October 2008, Dalian, China. Other presentations are published in this issue, pp. 1–347.
‡Corresponding author

lution method because the exact wave solutions to the frequency-domain governing differential equations are used as the frequency-dependent shape functions to formulate the exact dynamic stiffness matrix for a spectral element [11,12]. Thus, the SEM enables us to get very accurate dynamic response of a 1D structure by representing its regular structure members of any length (without any discontinuity or irregularity in geometrical and material properties) as one-element models. This can certainly benefit us to drastically reduce the computation cost and time.

As the applications of the SEM to the modeling and analysis of blood flow are very few, this paper first introduced a spectral element model for the blood flow through a human artery and then applied the spectral element model to some typical examples to investigate the blood flow characteristics in arteries.

GOVERNING EQUATIONS

1D theory of blood flow

The 1D theory of blood flow has been derived in a general form by Hughes and Lubliner [4], and it consists of a continuity equation, an axial momentum balance equation, and a constitutive equation for the flow of a Newtonian fluid in a deformable and impermeable, elastic tube. They are given by

Continuity equation:

$$\frac{\partial S}{\partial t}+\frac{\partial Q}{\partial x}=0 \tag{1}$$

Momentum balance equation:

$$\frac{\partial Q}{\partial t}+\frac{\partial}{\partial x}\left((1+\Lambda)\frac{Q^2}{S}\right)+\frac{S}{\rho}\frac{\partial P}{\partial x}=-\nu H\frac{Q}{S}+\nu\frac{\partial^2 Q}{\partial x^2} \tag{2}$$

Constitutive equation:

$$P(S(x,t),x,t)=P_d+\frac{4}{3}\frac{Eh}{r_d(x)}\left(1-\sqrt{\frac{S_d(x)}{S(x,t)}}\right) \tag{3}$$

where $Q(x,t)$ is the volumetric blood flow rate, $P(x,t)$ is the blood pressure, and $S(x,t)$ is the cross-sectional area of the artery. ρ is the mass density of blood, ν is the kinematic viscosity of blood, E is the Young's modulus of the artery, h is the wall thickness of the artery, and $S_d(x) = \pi r_d(x)^2$ is the cross-sectional wetted area where $r_d(x)$ is the inner radius of the artery at the diastole pressure P_d. Λ and H are the parameters determined by the flow velocity profiles across the cross-section and they are given by

$$\begin{aligned}
&\Lambda=0, \quad H=0 && \text{(Uniform flow)}\\
&\Lambda=\frac{1}{3}, \quad H=8\pi && \text{(Parabolic flow)}\\
&\Lambda=\frac{2\delta}{3R}, \quad H=\frac{2\pi R}{\delta} && \text{(Boundary layered flow)}
\end{aligned} \tag{4}$$

where the boundary layered (BL) flow means that the velocity profile is linear in the boundary layer of thickness δ and uniform in the core region. An empirical formula for Eh/r_d was derided by Olufsen [5] as

$$\frac{Eh}{r_d(x)}\cong\frac{Eh}{r_a}=k_1\exp(k_2 r_a)+k_3 \tag{5}$$

where $k_1 = 2 \times 10^7$ g s^{-2} cm^{-1}, $k_2 = -22.53$ cm^{-1}, $k_3 = 8.65 \times 10^5$ g s^{-2} cm^{-1}, and r_a is the mean radius of a tapered artery.

Linearized governing equations

Assume that the cross-sectional area of an artery varies slowly as follows:

$$S_d(x) = S_o(1 - \theta x) \qquad (\theta x < 1) \tag{6}$$

where $S_o = \pi r_o^2$ is the cross-sectional area at the artery inlet and θ is the parameter associated with the taper of artery. r_o is the inner radius at the artery inlet. The solutions of eqs. 1–3 are assumed in the perturbed forms as

$$\begin{aligned} Q(x, t) &= Q_d + q(x, t) \\ P(x, t) &= P_d + p(x, t) \\ S(x, t) &= S_d + s(x, t) \end{aligned} \tag{7}$$

where Q_d, P_d, and $S_d(x)$ are the blood flow rate, the blood pressure, and the cross-sectional wetted area at the diastole phase. $s(x,t)$ is the small perturbation with respect to $S_d(x)$ so that $s(x, t) < S_d(x)$. Applying eq. 7 to eq. 3 yields a relation as

$$s(x,t) = \frac{3}{2}\frac{r_a}{Eh} S_d(x)\, p(x,t) \tag{8}$$

where r_a is the mean inner radius of an artery. By substituting eqs. 7 into eqs. 1 and 2 and using eq. 8, we can obtain the linearized governing equations as

$$c_1 \dot{p} + q' = 0 \tag{9}$$

$$c_0 p' + \dot{q} + c_2 q + 2c_3 q' - c_4 q'' + c_5 = 0 \tag{10}$$

where

$$\begin{aligned} c_0 &= \frac{S_o}{\rho}, & c_1 &= \frac{3}{2}\frac{r_a}{Eh} S_o \\ c_2 &= \frac{\nu H}{S_o} + \frac{2(1+\Lambda)\theta}{S_o} Q_d, & c_3 &= \frac{1+\Lambda}{S_o} Q_d \\ c_4 &= \nu, & c_5 &= \frac{(1+\Lambda)\theta}{S_0} Q_d^2 + \frac{\nu H}{S_0} Q_d \end{aligned} \tag{11}$$

The derivative of eq. 10 with respect to x is given by

$$c_0 p'' + \dot{q}' + c_2 q' + 2c_3 q'' - c_4 q''' = 0 \tag{12}$$

From eq. 9, we get

$$q' = -c_1 \dot{p}, \quad \dot{q}' = -c_1 \ddot{p}, \quad q'' = -c_1 \dot{p}', \quad q''' = -c_1 \dot{p}'' \tag{13}$$

By using eq. 13, eq. 12 can be rewritten as

$$c_0 p'' - c_1 \ddot{p} - c_1 c_2 \dot{p} - 2c_1 c_3 \dot{p}' + c_1 c_4 \dot{p}'' = 0 \tag{14}$$

SPECTRAL ELEMENT MODELING

The individual arteries between any two neighboring bifurcating points can be represented by 1D spectral element models with specifying physiologically correct boundary conditions at their inlets and outlets. The finite spectral element model can be applied to most short arteries such as the aorta and iliac arteries (i.e., 4~6 cm). For a long artery such as femoral and brachial arteries (i.e., 38~45 cm), the finite spectral element can be applied to the short upstream part (computational domain) with large cross-sectional area, while the semi-infinite spectral element to the long downstream part with small cross-sectional area where the backward propagating blood waves reflected from the downstream end may be negligible. Thus, both finite and semi-infinite spectral elements are formulated in the following.

Finite spectral element

Governing equations in the frequency-domain

Based on the density functional theory (DFT) theory, we represent $p(x,t)$ and $q(x,t)$ in the spectral forms as

$$\begin{aligned} p(x,t) &= \frac{1}{N}\sum_{n=0}^{N-1} P_n(x)e^{i\omega_n t} \\ q(x,t) &= \frac{1}{N}\sum_{n=0}^{N-1} Q_n(x)e^{i\omega_n t} \end{aligned} \tag{15}$$

where $P_n(x)$ and $Q_n(x)$ are the spectral components of $p(x,t)$ and $q(x,t)$, respectively, and $\boldsymbol{P}$ and $\boldsymbol{Q}$ are defined by

$$\begin{aligned} \boldsymbol{P}(x) &= \{P_n(x);\ n = 0, 1, 2, \ldots, N-1\} \\ \boldsymbol{Q}(x) &= \{Q_n(x);\ n = 0, 1, 2, \ldots, N-1\} \end{aligned} \tag{16}$$

Substituting eq. 15 into eqs. 9 and eq. 14, we obtain

$$i\omega_n c_0 P_n + c_1 Q_n' = 0 \tag{17}$$

$$P_n''(x) - 2b_{1n}P_n'(x) + b_{2n}P_n(x) = 0 \tag{18}$$

where

$$\begin{aligned} b_{1n} &= \frac{c_1^2 c_3 c_4 \omega_n^2 + i c_0 c_1 c_3 \omega_n}{c_0^2 + c_1^2 c_4^2 \omega_n^2} \\ b_{2n} &= \omega_n^2 \frac{c_0 c_1 - c_1^2 c_2 c_4}{c_0^2 + c_1^2 c_4^2 \omega_n^2} - i\omega_n \frac{c_0 c_1 c_2 + c_1^2 c_4 \omega_n^2}{c_0^2 + c_1^2 c_4^2 \omega_n^2} \end{aligned} \tag{19}$$

Weak form of governing equations

The weak form of eq. 18 can be derived from

$$\int_0^L [P_n''(x) - 2b_{1n}P_n'(x) + b_{2n}P_n(x)]\delta P_n(x)\,dx = 0 \tag{20}$$

where the subscripts n are omitted for the brevity.

By applying the integral by parts, we can obtain

$$\begin{aligned}\int_0^L P_n''(x)\delta P_n(x)\,dx &= P_n'(x)\delta P_n(x)\Big|_0^L - \int_0^L P_n'(x)\delta P_n'(x)\,dx \\ \int_0^L P_n'(x)\delta P_n(x)\,dx &= P_n(x)\delta P_n(x)\Big|_0^L - \int_0^L P_n(x)\delta P_n'(x)\,dx\end{aligned} \tag{21}$$

Applying eq. 13 to eq. 10 yields

$$p' = -\frac{1}{c_0}\dot{q} - \frac{c_2}{c_0}q + 2\frac{c_1c_3}{c_0}\dot{p} - \frac{c_1c_4}{c_0}\dot{p}' - \frac{c_5}{c_0} \tag{22}$$

By using eq. 15, eq. 22 can be transformed in the frequency-domain as

$$P_n' = -\frac{i\omega_n + c_2}{c_0}Q_n + 2\frac{i\omega_n c_1c_3}{c_0}P_n - \frac{i\omega_n c_1c_4}{c_0}P_n' - \frac{c_5}{c_0}C_{0n} \tag{23}$$

or

$$P_n' = -i\omega_n a_{1n}Q_n - a_{2n}Q_n + a_{3n}P_n - a_{4n}C_{0n} \tag{24}$$

where

$$\begin{aligned}a_{1n} &= \frac{1}{c_0 + ic_1c_4\omega_n}, & a_{2n} &= \frac{c_2}{c_0 + ic_1c_4\omega_n} \\ a_{3n} &= \frac{2ic_1c_3\omega_n}{c_0 + ic_1c_4\omega_n} = 2b_{1n}, & a_{4n} &= \frac{c_5}{c_0 + ic_1c_4\omega_n}\end{aligned} \tag{25}$$

and

$$C_{0n} = N\delta_{0n} = \begin{cases} N & \text{if } n = 0 \\ 0 & \text{otherwise}\end{cases} \tag{26}$$

By substituting eq. 24 into the first term in the right-hand side of eq. 21a, we obtain

$$\int_0^L P_n''(x)\delta P_n\,dx = (-i\omega_n a_{1n}Q_n - a_{2n}Q_n + a_{3n}P_n)\delta P_n(x)\Big|_0^L - \int_0^L P_n'(x)\delta P_n'(x)\,dx \tag{27}$$

Finally, by replacing the first term of eq. 20 with eq. 27, we can obtain the weak form in the frequency-domain as

$$\begin{aligned}&\alpha_{1n}\int_0^L P_n'(x)\delta P_n'(x)\,dx + \alpha_{2n}\int_0^L [P_n'(x)\delta P_n(x) - P_n(x)\delta P_n'(x)]\,dx \\ &- \alpha_{3n}\int_0^L P_n(x)\delta P_n(x)\,dx = -\bar{\alpha}_{4n}Q_n(x)\delta P_n(x)\Big|_0^L \\ &- Q_n(x)\delta P_n(x)\Big|_0^L + \alpha_{2n}P_n(x)\delta P_n(x)\Big|_0^L - \alpha_{5n}\delta P_n(x)\Big|_0^L\end{aligned} \tag{28}$$

where

$$\alpha_{1n} = \frac{1}{a_{2n}} = \frac{c_0 + i\omega_n c_1 c_4}{c_2}, \qquad \alpha_{2n} = \frac{b_{1n}}{a_{2n}} = \frac{i\omega_n c_1 c_3}{c_2}$$
$$\alpha_{3n} = \frac{b_{2n}}{a_{2n}} = \omega_n^2 \frac{c_0 c_1 - c_1^2 c_2 c_4}{c_2(c_0 - ic_1 c_4 \omega_n)} - i\omega_n \frac{c_0 c_1 c_2 + c_1^2 c_4 \omega_n^2}{c_2(c_0 - ic_1 c_4 \omega_n)} \tag{29}$$
$$\bar{\alpha}_{4n} = \frac{i\omega_n a_{1n}}{a_{2n}} = \frac{i\omega_n}{c_2}, \qquad \alpha_{5n} = \frac{a_{4n}}{a_{2n}} C_{0n} = \frac{c_5}{c_2} C_{0n}$$

Spectral nodal degrees-of-freedom (DOFs)

Consider a finite artery element of length L and assume that $x = 0$ and $x = L$ denote the upstream end and downstream end of the artery element, respectively. Then we define the spectral nodal DOFs vectors for the blood flow rate and pressure as follows:

$$\boldsymbol{P}_n = \begin{Bmatrix} P_{n1} \\ P_{2n} \end{Bmatrix} = \begin{Bmatrix} +P_n(0) \\ +P_n(L) \end{Bmatrix} \tag{30}$$

$$\boldsymbol{Q}_n = \begin{Bmatrix} Q_{1n} \\ Q_{2n} \end{Bmatrix} = \begin{Bmatrix} +Q_n(0) \\ -Q_n(L) \end{Bmatrix} \tag{31}$$

Dynamic shape functions

To derive the frequency-dependent dynamic shape functions, we assume the general solution of eq. 18 as

$$P_n(x) = ae^{-ik_n x} \tag{32}$$

where k_n is the wave number. Substituting eq. 32 into eq. 18, we get a dispersion relation

$$k_n^2 - 2ib_{1n}k_n - b_{2n} = 0 \tag{33}$$

From eq. 33, we can obtain two wavenumbers as

$$k_{n1} = ib_{1n} + \sqrt{-b_{1n}^2 + b_{2n}}, \qquad k_{n2} = ib_{1n} - \sqrt{-b_{1n}^2 + b_{2n}} \tag{34}$$

If the artery is uniform ($\theta = 0$) and the blood is non-viscid ($\nu = 0$), k_{n1} represents a wave mode which travels in the $+x$ direction without attenuation (forward propagating wave) while k_{n2} a wave mode which travels in the $-x$ direction without attenuation (backward propagating wave). However, as the arteries are not uniform ($\theta \neq 0$) and the bloods are viscid ($\nu \neq 0$) in real situations, both wavenumbers k_{n1} and k_{n2} will be complex with imaginary values. This means that k_{n1} and k_{n2} represent the wave modes which attenuate as they travel in the $+x$ and $-x$ directions, respectively.

By using the wavenumbers, the general solution of eq. 18 can be written as

$$P_n(x) = \boldsymbol{e}_n(x)\boldsymbol{a} \tag{35}$$

where

$$\boldsymbol{e}_n(x) = \begin{bmatrix} e^{-ik_{n1}x} & e^{-ik_{n2}x} \end{bmatrix} \tag{36}$$

and

$$\boldsymbol{a} = \{a_1 \;\; a_2\}^{\mathrm{T}} \tag{37}$$

By applying eq. 35 to the right-hand side of eq. 30, we can obtain

$$\boldsymbol{P}_n = \boldsymbol{H}_n(\omega_n)\boldsymbol{a} \tag{38}$$

where

$$\boldsymbol{H}_n(\omega_n) = \begin{bmatrix} 1 & 1 \\ e^{-ik_{n1}L} & e^{-ik_{n2}L} \end{bmatrix} \tag{39}$$

By using eq. 38, the constant vector $\boldsymbol{a}$ can be removed from eq. 35 to obtain

$$P_n(x) = \boldsymbol{N}_n(x;\, \omega_n)\boldsymbol{P}_n \tag{40}$$

where $\boldsymbol{N}_n(x;\, \omega_n)$ is the dynamic shape function defined by

$$\begin{aligned} \boldsymbol{N}_n(x;\omega_n) &= \boldsymbol{e}_n(x)\boldsymbol{H}_n(\omega_n)^{-1} \\ &= \frac{1}{\Delta_n}[e^{-i(k_{n1}x+k_{n2}L)} - e^{-i(k_{n2}x+k_{n1}L)} \qquad e^{-ik_{n2}x} - e^{-ik_{n1}x} \;\;] \end{aligned} \tag{41}$$

where

$$\Delta_n = e^{-ik_{n2}L} - e^{-ik_{n1}L} \tag{42}$$

Spectral element equation

By using the spectral nodal DOFs defined by eqs. 30 and 31, the weak form of eq. 28 can be rewritten as

$$\begin{aligned} &\alpha_{1n}\textstyle\int_0^L P_n'(x)\,\delta P_n'(x)\,dx + \alpha_{2n}\int_0^L [P_n'(x)\,\delta P_n(x) - P_n(x)\,\delta P_n'(x)]\,dx \\ &- \alpha_{3n}\textstyle\int_0^L P_n(x)\,\delta P_n(x)\,dx = \bar{\alpha}_{4n}\delta \boldsymbol{P}_n^{\mathrm{T}}\boldsymbol{Q}_n + \delta \boldsymbol{P}_n^{\mathrm{T}}\boldsymbol{Q}_n + \alpha_{2n}\delta \boldsymbol{P}_n^{\mathrm{T}}\boldsymbol{T}\boldsymbol{P}_n + \alpha_{5n}\delta \boldsymbol{P}_n^{\mathrm{T}}\mathbf{U} \end{aligned} \tag{43}$$

where

$$\boldsymbol{T} = \begin{bmatrix} -1 & 0 \\ 0 & 1 \end{bmatrix}, \; \boldsymbol{U} = \begin{Bmatrix} 1 \\ -1 \end{Bmatrix} \tag{44}$$

The weak form of eq. 17 can be written as

$$\textstyle\int_0^L (ic_1\omega_n P_n + Q_n')\delta Q_n(x)\,dx = 0 \tag{45}$$

From the linear homogenous wave equation for $Q_n(x)$, which has the same form as eq. 18, we can derive

$$Q_n(x) = \boldsymbol{N}_n(x;\omega_n)\boldsymbol{Q}_n \tag{46}$$

By substituting eqs. 40 and 46 into eq. 45, we can obtain a complementary equation as

$$\boldsymbol{Q}_n = -ic_1\omega_n \boldsymbol{R}_n \boldsymbol{P}_n \tag{47}$$

where

$$\boldsymbol{R}_n = \frac{1}{\Delta_n k_{n1} k_{n2}} \begin{bmatrix} -ik_{n1}e_{n1} + ik_{n2}e_{n2} & ik_{n1} - ik_{n2} \\ e_{n1}e_{n2}(-ik_{n1} + ik_{n2}) & ik_{n1}e_{n2} - ik_{n2}e_{n1} \end{bmatrix} \tag{48}$$

with

$$\Delta_n = e_{n2} - e_{n1}, \quad e_{n1} = e^{-ik_{n1}L}, \quad e_{n2} = e^{-ik_{n2}L} \tag{49}$$

Substituting eq. 40 into eq. 43 and applying eq. 47 to the first term in the right-hand side of eq. 43 yields

$$\begin{aligned} &\delta \boldsymbol{P}_n^{\mathrm{T}} [\alpha_{1n} \textstyle\int_0^L \boldsymbol{N}_n'^{\mathrm{T}} \boldsymbol{N}_n' \, dx + \alpha_{2n} (\int_0^L \boldsymbol{N}_n^{\mathrm{T}} \boldsymbol{N}_n' \, dx - \int_0^L \boldsymbol{N}_n'^{\mathrm{T}} \boldsymbol{N}_n \, dx) \\ &- \alpha_{3n} \textstyle\int_0^L \boldsymbol{N}_n^{\mathrm{T}} \boldsymbol{N}_n \, dx - \alpha_{4n} \boldsymbol{R}_n - \alpha_{2n} \boldsymbol{T}] \boldsymbol{P}_n = \delta \boldsymbol{P}_n^{\mathrm{T}} [\boldsymbol{Q}_n + \alpha_{5n} \boldsymbol{U}] \end{aligned} \tag{50}$$

where

$$\alpha_{4n} = \alpha_{4n}(-ic_1\omega_n) = \frac{c_1}{c_2}\omega_n^2 \tag{51}$$

Since $\delta \boldsymbol{P}_n$ is the arbitrary variation of $\boldsymbol{P}_n$, we obtain from eq. 50

$$\boldsymbol{S}(\omega_n)\boldsymbol{P}_n = \boldsymbol{Q}_n \tag{52}$$

where

$$\begin{aligned} \boldsymbol{S}(\omega_n) = {} & \alpha_{1n} \textstyle\int_0^L \boldsymbol{N}_n'^{\mathrm{T}} \boldsymbol{N}_n' \, dx + \alpha_{2n} (\int_0^L \boldsymbol{N}_n^{\mathrm{T}} \boldsymbol{N}_n' \, dx - \int_0^L \boldsymbol{N}_n'^{\mathrm{T}} \boldsymbol{N}_n \, dx) \\ & - \alpha_{3n} \textstyle\int_0^L \boldsymbol{N}_n^{\mathrm{T}} \boldsymbol{N}_n \, dx - \alpha_{4n} \boldsymbol{R}_n - \alpha_{2n} \boldsymbol{T} \end{aligned} \tag{53}$$

By substituting the dynamic shape function eq. 41 into eq. 53 and taking integration, we obtain the spectral element matrix as

$$\boldsymbol{S}(\omega_n) = \frac{1}{\Delta_n^2} \begin{bmatrix} S_{n11} & S_{n12} \\ S_{n21} & S_{n22} \end{bmatrix} - \alpha_{4n} \boldsymbol{R}_n - \alpha_{2n} \boldsymbol{T} \tag{54}$$

where

$$\begin{aligned} S_{n11} &= i\beta_{n1}\lambda_{n1}\varepsilon_{n1}e_{n2}^2 + i\beta_{n2}\lambda_{n2}\varepsilon_{n2}e_{n1}^2 - \beta_{n3}(\lambda_{n3} + \lambda_{n4})\varepsilon_{n3}e_{n1}e_{n2} \\ S_{n12} &= -i\beta_{n1}\lambda_{n1}\varepsilon_{n1}e_{n2} - i\beta_{n2}\lambda_{n2}\varepsilon_{n2}e_{n1} + \beta_{n3}\varepsilon_{n3}(\lambda_{n3}e_{n2} + \lambda_{n4}e_{n1}) \\ S_{n21} &= -i\beta_{n1}\lambda_{n1}\varepsilon_{n1}e_{n2} - i\beta_{n2}\lambda_{n2}\varepsilon_{n2}e_{n1} + \beta_{n3}\varepsilon_{n3}(\lambda_{n3}e_{n1} + \lambda_{n4}e_{n2}) \\ S_{n22} &= i\beta_{n1}\lambda_{n1}\varepsilon_{n1} + i\beta_{n2}\lambda_{n2}\varepsilon_{n2} - \beta_{n3}(\lambda_{n3} + \lambda_{n4})\varepsilon_{n3} \end{aligned} \tag{55}$$

with

$$\begin{aligned}
&\beta_{n1} = (1/2)k_{n1}^{-1}, \quad \beta_{n2} = (1/2)k_{n2}^{-1}, \quad \beta_{n3} = (k_{n1} + k_{n2})^{-1} \\
&\varepsilon_{n1} = 1 - e_{n1}^2, \quad \varepsilon_{n2} = 1 - e_{n2}^2, \quad \varepsilon_{n3} = 1 - e_{n1}e_{n2} \\
&\lambda_{h1} = \alpha_{1n}k_{n1}^2 + \alpha_{3n} \\
&\lambda_{h2} = \alpha_{1n}k_{n2}^2 + \alpha_{3n} \\
&\lambda_{h3} = i\alpha_{1n}k_{n1}k_{n2} + (k_{n1} - k_{n2})\alpha_{2n} + i\alpha_{3n} \\
&\lambda_{h4} = i\alpha_{1n}k_{n1}k_{n2} + (k_{n2} - k_{n1})\alpha_{2n} + i\alpha_{3n}
\end{aligned} \tag{56}$$

Semi-infinite spectral element

To formulate the spectral element for a semi-infinite blood flow element, we start again from eqs. 9 and 10. The governing equations are represented in the spectral forms as

$$ic_1\omega_n P_n(x) + Q_n'(x) = 0 \tag{57}$$

$$c_0 P_n'(x) + i\omega_n Q_n(x) + c_2 Q_n(x) + 2c_3 Q_n'(x) - c_4 Q_n''(x) + c_5 = 0 \tag{58}$$

From eqs. 57 and 58, we can obtain the wave equation for $Q_n(x;\,)$ as

$$Q_n''(x) - 2b_{1n}Q_n'(x) + b_{2n}Q_n(x) = 0 \tag{59}$$

where b_{1n} and b_{2n} are defined by eq. 19. Assume the general solution of eq. 59 as

$$Q_n(x) = ae^{-ik_n x} \tag{60}$$

Substituting eq. 60 into eq. 59 yields a dispersion relation as

$$k_n^2 - 2ib_{1n}k_n - b_{2n} = 0 \tag{61}$$

As eq. 59 for $Q_n(x)$ has the exactly same form as eq. 18 for $P_n(x)$, we get an dispersion relation (eq. 61) that is identical to eq. 33. Accordingly, we also obtain two identical wavenumbers k_{n1} and k_{n2} given by eq. 34. The wavenumber k_{n1} corresponds to the wave which is propagating in the $+x$ direction (the forward-propagating wave mode), while the wavenumber k_{n1} corresponds to the wave which is propagating in the $-x$ direction (the backward-propagating wave mode).

For the blood flow through a very long blood vessel, we may assume that the blood wave propagates forward only so that the backward-propagating waves reflected from the far downstream can be neglected. This approximation may lead to a nonresonant single-node semi-infinite spectral element. Thus, we represent the blood flow rate as

$$Q_n(x) = ae^{-ik_{n1}x} \tag{62}$$

The spectral nodal DOFs at the upstream end (inlet) of a semi-infinite blood vessel element are defined by

$$Q_n(0) = Q_{n1}, \qquad P_n(0) = P_{n1} \tag{63}$$

By using the first relation of eq. 63, eq. 62 can be written as

$$Q_n(x) = e^{-ik_{n1}x}Q_{n1} \tag{64}$$

Substituting eq. 64 into the continuity eq. 57, we obtain

$$P_n(x) = \frac{k_{n1}}{c_1 \omega_n} Q_{n1} e^{-ik_{n1}x} \tag{65}$$

Lastly, applying the second relation of eq. 63 to eq. 65, we obtain the semi-infinite spectral element equation as

$$S_n^{SI} P_{n1} = Q_{n1} \tag{66}$$

where

$$S_n^{SI} = c_1 \frac{\omega_n}{k_{n1}} \tag{67}$$

ASSEMBLY OF SPECTRAL ELEMENTS

The spectral elements can be assembled in the same way as used in the conventional FEM. The assembling is straightforward for straight blood vessels. Thus, the assembly process will be illustrated for the case of a binary branch which consists of a parent vessel (denoted by "p") and two daughter vessels (denoted by "d_1" and "d_2") as shown in Fig. 1.

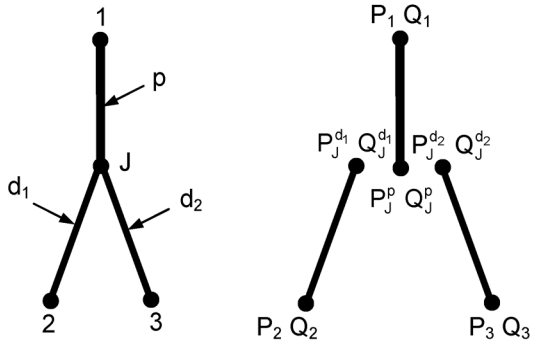

Fig. 1 A binary branch vessel.

At the bifurcation point "J", the following bifurcation conditions must be satisfied.

$$P_J^p = P_J^{d_1} = P_J^{d_2} = P_J \tag{68}$$

$$Q_J^p = Q_J^{d_1} + Q_J^{d_2} \tag{69}$$

The spectral element equations for the parent vessel and two daughter vessels are given by

$$\begin{bmatrix} S^p_{n11} & S^p_{n12} \\ S^p_{n21} & S^p_{n22} \end{bmatrix} \begin{Bmatrix} P_1 \\ P^p_J \end{Bmatrix} = \begin{Bmatrix} Q_1 \\ Q^p_J \end{Bmatrix} \text{(parent)}$$

$$\begin{bmatrix} S^{d_1}_{n11} & S^{d_1}_{n12} \\ S^{d_1}_{n21} & S^{d_1}_{n22} \end{bmatrix} \begin{Bmatrix} P^{d1}_J \\ P_2 \end{Bmatrix} = \begin{Bmatrix} Q^{d_1}_J \\ Q_2 \end{Bmatrix} \text{(daughter 1)} \tag{70}$$

$$\begin{bmatrix} S^{d_2}_{n11} & S^{d_2}_{n12} \\ S^{d_2}_{n21} & S^{d_2}_{n22} \end{bmatrix} \begin{Bmatrix} P^{d_2}_J \\ P_3 \end{Bmatrix} = \begin{Bmatrix} Q^{d_2}_J \\ Q_3 \end{Bmatrix} \text{(daughter 2)}$$

where the nonlinear pseudo forces are omitted for brevity. By using the bifurcation conditions (eq. 68) and (eq. 69), three spectral element equations (eq. 58) can be readily assembled in the form as

$$\begin{bmatrix} S^p_{n11} & S^p_{n12} & 0 & 0 \\ S^p_{n21} & S^p_{n22} + S^{d_1}_{n11} + S^{d_2}_{n11} & S^{d_1}_{n12} & S^{d_2}_{n12} \\ 0 & S^{d_1}_{n21} & S^{d_1}_{n22} & 0 \\ 0 & S^{d_2}_{n21} & 0 & S^{d_2}_{n22} \end{bmatrix} \begin{Bmatrix} P_1 \\ P_J \\ P_2 \\ P_3 \end{Bmatrix} = \begin{Bmatrix} Q_1 \\ 0 \\ Q_2 \\ Q_3 \end{Bmatrix} \tag{71}$$

NUMERICAL EXAMPLES AND DISCUSSION

The spectral element model developed in this paper is applied to a blood vessel as shown in Fig. 2, where the inlet radius is $r_0 = 1.25$ cm and the taper is $\theta = 0.018$ for the short upstream part (10 cm) and $\theta = 0$ for the long downstream part (2490 cm). The long uniform downstream part is attached to the short tapered upstream part to resemble Aorta and the rest downstream part connected to Aorta. The blood properties are given by $\rho = 1.055$ g/cm^3 and $\nu = 0.046$ cm^2/s. The blood flow rate and pressure are computed by assuming that the pulsatile blood flow rate at the upstream inlet ($x = 0$ cm) and the pulsatile blood pressure at the downstream outlet are given by Fig. 3.

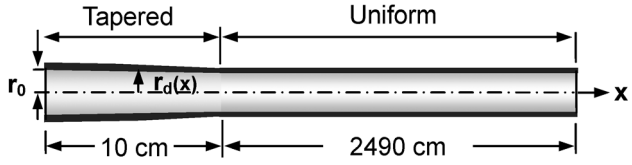

Fig. 2 An example blood vessel.

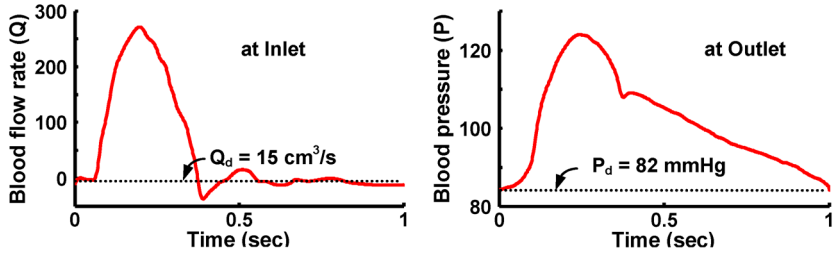

Fig. 3 Inlet and outlet boundary conditions of the blood flow.

First, to evaluate the high accuracy of the present spectral element model, the blood flow rate and pressure predicted by using the present spectral element model are compared with those predicted by using the finite element model formulated in this study. The velocity profile of the blood flow is assumed to be parabolic. Figure 4 shows the predictions at $x = 3.5$ cm. For the SEM results, only two spectral elements are used: one element for the short tapered upstream part and one element for the rest long uniform downstream part. For the FEM results, the short tapered upstream part is represented by total 10 equal-length elements and the rest long uniform downstream part is represented by total 10, 40, 90, or 190 equal-length elements. The Runge–Kutta algorithm is applied to compute the FEM results, with using the time-step size of 0.01 s which is confirmed to provide sufficiently converged reliable solutions. Figure 4 certainly shows that FEM results converge to the SEM results as the number of finite elements used in FEM is increased. Figure 4 also shows that, as the blood flow specified at the inlet and outlet boundaries is pulsatile, the blood flow predicted at $x = 5$ cm is also pulsatile as expected. The blood flow rates and pressures at three different locations are compared in Fig. 5. Figure 5 shows the slight time delays of the blood flow waves depending on the measurement locations.

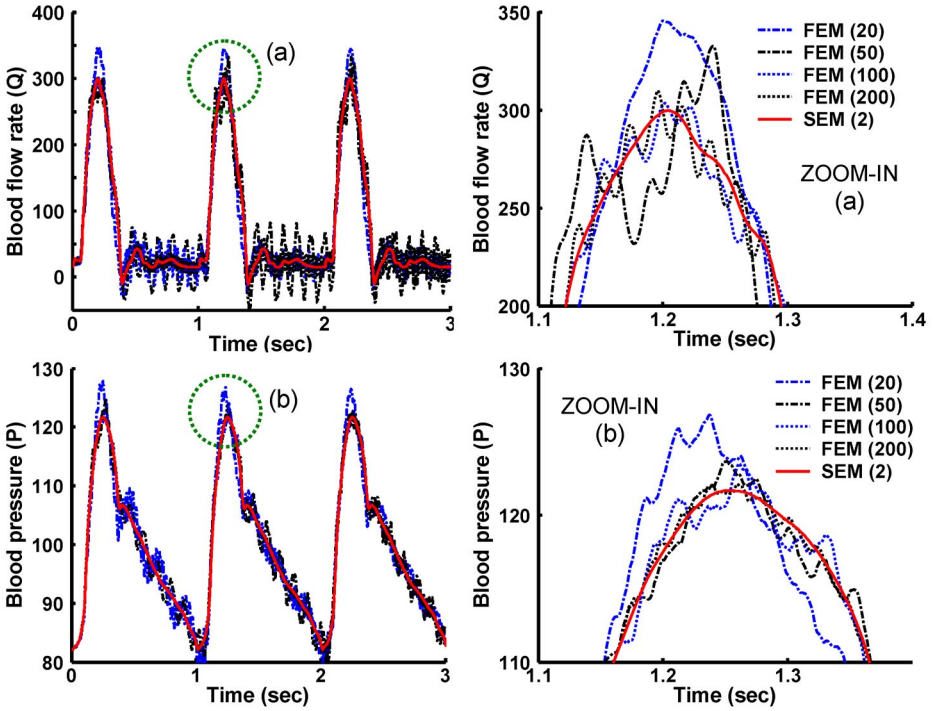

Fig. 4 Comparison of the blood flow rates and pressures obtained by SEM and FEM.

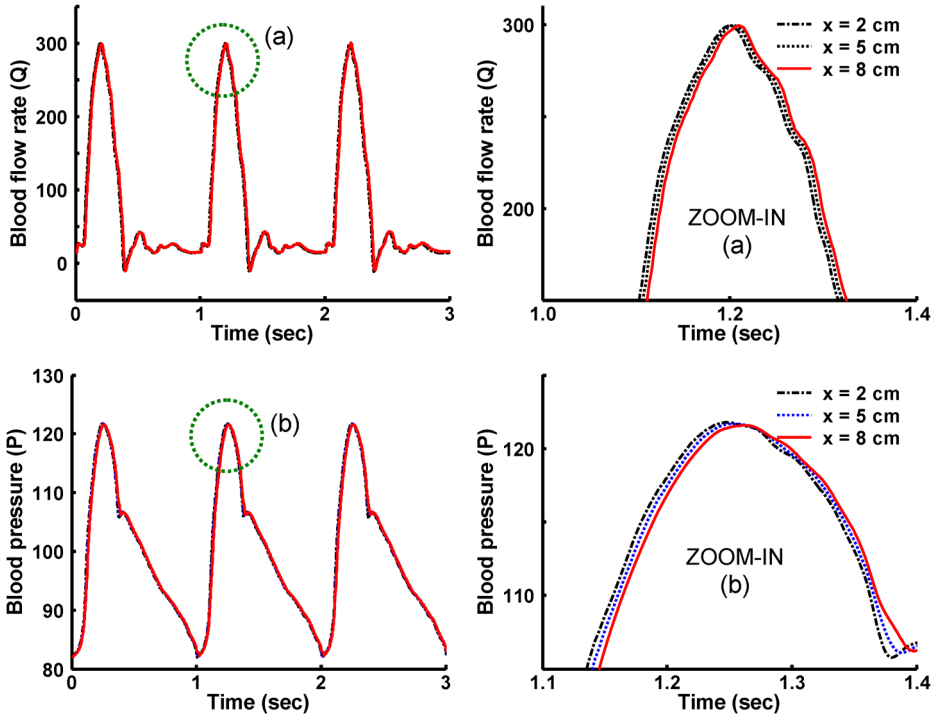

Fig. 5 Blood flow rates and pressures at various locations.

The blood flow characteristics in a blood vessel will depend on the velocity profile which is determined by the blood properties (i.e., viscosity, density, etc.) and the geometric and material properties of the blood vessel. Thus, we consider three types of velocity profile: the uniform flow, the parabolic flow, and the BL flow. The blood flow rates and pressures predicted at $x = 5$ cm for each velocity profile are compared in Fig. 6. For the BL flow, 5 % BL thickness is assumed. Figure 6 shows that the uniform flow has the largest blood flow rate while the BL flow has the lowest value.

In this study, the nonlinear blood flow theory is linearized by neglecting small nonlinear terms from eq. 14. By taking into account the neglected nonlinear terms as the nonlinear pseudo-forces, the spectral element analysis can be also conducted by using the present spectral element model. To evaluate the effect of the nonlinear terms, the blood flow rates and pressures predicted by using the linear and nonlinear spectral element analyses are compared in Fig. 7. It is shown that the linear spectral element analysis is good enough for the example problem considered in this study.

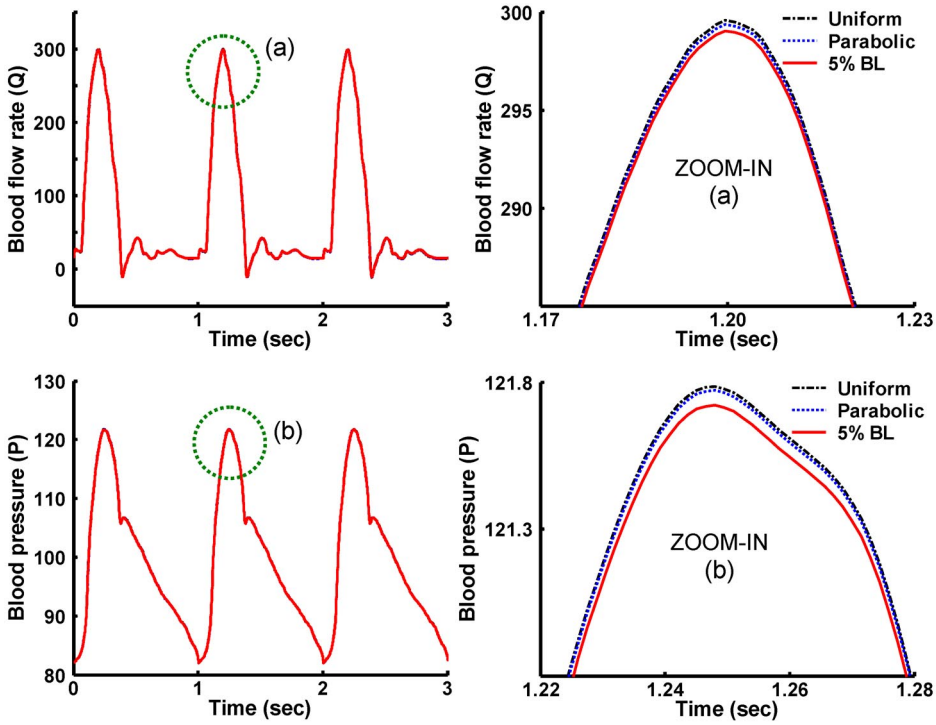

Fig. 6 Blood flow rate and pressure vs. blood flow velocity profile.

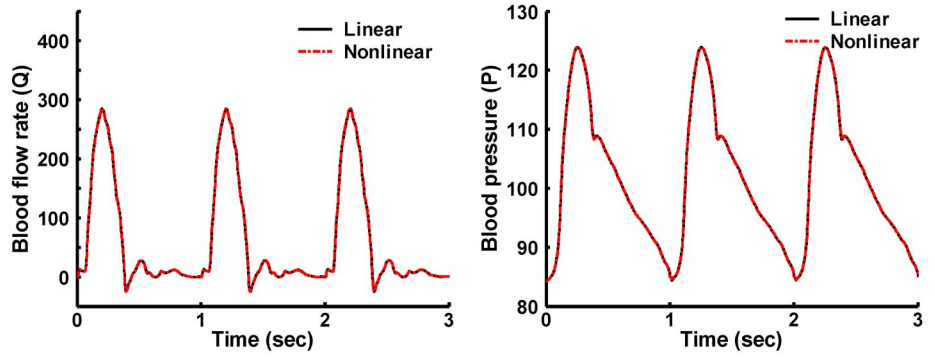

Fig. 7 Comparison of the linear and nonlinear blood flow models.

As the second example, we consider the artery system that consists of the subclavian, vertebral artery, and brachial artery as shown in Fig. 8. The geometric data of the artery system is available from ref. [14]. The semi-infinite spectral elements are used to represent the non-reflecting boundary conditions at the downstream ends of the vertebral artery and brachial artery. Figure 9 shows the blood flow rates and pressures predicted at the 2 cm distance from the inlet of subclavian (location A), at the 5 cm distance from the junction J of the vertebral artery (location B), and at the 20 cm distance from the junction J of the brachial artery (location C). As expected, the blood flow rate at B is shown to be smaller than the value at C, while the blood pressures are almost same at three locations.

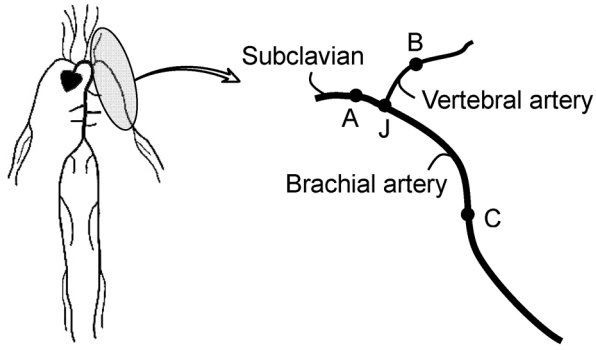

Fig. 8 Artery system considered as the second example.

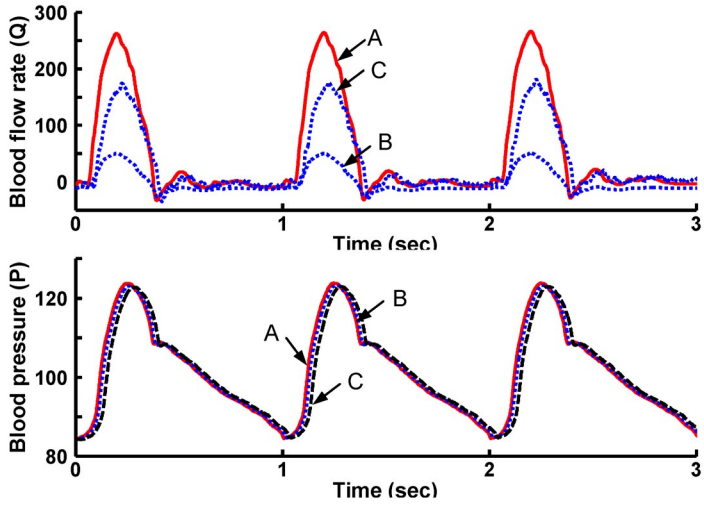

Fig. 9 Blood flow rates and pressures at location A, B, and C.

CONCLUSIONS

In this paper, a 1D spectral element model for the blood flows in the human arteries with varying cross-sections is developed by using the variational approach. By suing the exact wave solutions to the frequency-domain governing differential equations as the frequency-dependent shape functions, both the finite spectral element and the semi-infinite spectral element are formulated. Through some numeral simulations, it is shown that the present spectral element model provides very accurate and reliable solutions, with using only a small number of elements, when compared with the conventional finite element model.

APPENDIX: FINITE ELEMENT MODEL

The weak form of the time-domain governing eq. 14 is obtained from

$$\int_0^L [c_0 p'' - c_1 \ddot{p} - c_1 c_2 \dot{p} - 2c_1 c_3 \dot{p}' + c_1 c_4 \dot{p}''] \delta p \, dx = 0 \tag{A1}$$

By applying the integral by parts and using eqs. 13 and 22, we obtain the weak form as

$$\begin{aligned} &c_1 c_2^{-1} \int_0^L \ddot{p} \delta p \, dx + c_1 \int_0^L \dot{p} \delta p \, dx + c_1 c_2^{-1} c_3 \left(\int_0^L \dot{p}' \delta p \, dx - \int_0^L \dot{p} \delta p' \, dx\right) \\ &+ c_1 c_2^{-1} c_4 \int_0^L \dot{p}' \delta p' \, dx + c_0 c_2^{-1} \int_0^L p' \delta p' \, dx = (-c_2^{-1} \dot{q} - q + c_1 c_2^{-1} c_3 \dot{p} - c_2^{-1} c_5) \delta p \Big|_0^L \end{aligned} \tag{A2}$$

For the three-node element, the blood flow rate and pressure are assumed by

$$p(x,t) = \boldsymbol{N}_p(x)\boldsymbol{p}(t), \qquad q(x,t) = \boldsymbol{N}_q(x)\boldsymbol{q}(t) \tag{A3}$$

where

$$\begin{aligned} \boldsymbol{p}(t) &= \{p_1(t) \;\; p_2(t) \;\; p_3(t)\}^{\mathrm{T}} = \{p(0,t) \;\; p(L/2,t) \;\; p(L,t)\}^{\mathrm{T}} \\ \boldsymbol{q}(t) &= \{q_1(t) \;\; q_3(t)\}^{\mathrm{T}} = \{q(0,t) \;\; q(L,t)\}^{\mathrm{T}} \end{aligned} \tag{A4}$$

and

$$\begin{aligned} \boldsymbol{N}_p(x) &= \; [1 - 3\xi + 2\xi^2 \quad 4\xi - 4\xi^2 \quad -\xi + 2\xi^2] \\ \boldsymbol{N}_q(x) &= \; [1 - 3\xi + 2\xi^2 \quad \xi - 2\xi^2] \\ \xi &= x / L \end{aligned} \tag{A5}$$

The weak form of eq. 9 is written as

$$\int_0^L (c_1 \dot{p} + q') \delta q \, dx = 0 \tag{A6}$$

Substitution of eq. A3 into eq. A6 yields a complementary relation as

$$\boldsymbol{q} = -c_1 \boldsymbol{R}_1 \dot{\boldsymbol{p}} \tag{A7}$$

where

$$\boldsymbol{R}_1 = -\frac{L}{40}\begin{bmatrix} 11 & 8 & 1 \\ 1 & 8 & 11 \end{bmatrix} \tag{A8}$$

By substituting eq. A3 into eq. A2 and using the complementary relation (A7), we obtain the finite element equation in the form as

$$\boldsymbol{M}\ddot{\boldsymbol{p}} + \boldsymbol{C}\dot{\boldsymbol{p}} + \boldsymbol{K}\boldsymbol{p} = \boldsymbol{q} + \boldsymbol{f}_C \tag{A9}$$

where

$$\begin{aligned}
\boldsymbol{M} &= c_1 c_2^{-1} \int_0^L \boldsymbol{N}_p(x)^{\mathrm{T}} \boldsymbol{N}_p(x)\, dx + c_1 c_2^{-1} \boldsymbol{R}_2 \\
\boldsymbol{C} &= c_1 \int_0^L \boldsymbol{N}_p(x)^{\mathrm{T}} \boldsymbol{N}_p(x)\, dx + c_1 c_2^{-1} c_3 \int_0^L [\boldsymbol{N}_p(x)^{\mathrm{T}} \boldsymbol{N}'_p(x) - \boldsymbol{N}'_p(x)^{\mathrm{T}} \boldsymbol{N}_p(x)]\, dx \\
&\quad + c_1 c_2^{-1} c_4 \int_0^L \boldsymbol{N}'_p(x)^{\mathrm{T}} \boldsymbol{N}'_p(x)\, dx - c_1 c_2^{-1} c_3\, \boldsymbol{N}_p^{\mathrm{T}}(x) \boldsymbol{N}_p(\boldsymbol{x}) \Big|_0^L \\
\boldsymbol{K} &= c_0 c_2^{-1} \int_0^L \boldsymbol{N}'_p(x)^{\mathrm{T}} \boldsymbol{N}'_p(x)\, dx
\end{aligned} \tag{A9}$$

and

$$\begin{aligned}
\boldsymbol{q} &= -\boldsymbol{N}_p^{\mathrm{T}}(x) \boldsymbol{N}_q(x) \Big|_0^L \quad \boldsymbol{q} = \{q_1 \;\; 0 \;\; q_2\}^{\mathrm{T}} \\
\boldsymbol{f}_C &= -c_2^{-1} c_5\, \boldsymbol{N}_p(x) \Big|_0^L = c_2^{-1} c_5 \{1 \;\; 0 \;\; -1\}^{\mathrm{T}}
\end{aligned} \tag{A10}$$

with

$$\boldsymbol{R}_2 = -\frac{L}{40} \begin{bmatrix} 11 & 8 & 1 \\ 0 & 0 & 0 \\ 1 & 8 & 11 \end{bmatrix} \tag{A111}$$

REFERENCES

1. N. Westerhof, F. Bosman, C. J. De Vries. *J. Biomech.* **2**, 121 (1969).
2. R. Pietrabissa, S. Mantero, T. Marotta, S. Menicanti. *Med. Eng. Phys.* **18**, 477 (1996).
3. J. R. Womersley. *Phys. Med. Biol.* **2**, 178 (1957).
4. T. J. R. Hughes, J. Lubliner. *Math. Biosci.* **18**, 161 (1973).
5. M. S. Olufsen. *Am. J. Physiol.* **276**, H257 (1999).
6. B. N. Steele, J. Wan, J. P. Ku, T. J. R. Hughes, C. A. Taylor. *IEEE Trans. Biomed. Eng.* **50**, 649 (2003).
7. C. A. Taylor, T. J. R. Hughes, C. K. Zarins. *Ann. Biomed. Eng.* **26**, 975 (1998).
8. L. Formaggia, J. F. Gerbeau, F. Nobile, A. Quarteroni. *Comput. Meth. Appl. Mech. Eng.* **191**, 561 (2001).
9. J. P. Ku, M. T. Draney, F. R. Arko, W. A. Lee, F. P. Chan, N. J. Pelc, C. K. Zarins, C. A. Taylor. *Ann. Biomed. Eng.* **30**, 743 (2002).
10. K. Laganà, G. Dubini, F. Migliavacca, R. Pietrabissa, G. Pennati, A. Veneziani, A. Quarteroni. *Biorheorogy* **39**, 359 (2002).
11. J. F. Doyle. *Wave Propagation in Structures: Spectral Analysis Using Fast Discrete Fourier Transforms*, Springer, New York (1997).
12. U. Lee. *Spectral Element Method in Structural Dynamics*, John Wiley, Singapore (2009).
13. D. E. Newland. *Random Vibrations, Spectral and Wavelet Analysis*, Longman, New York (1993).
14. J. T. Ottesen, M. S. Olufsen, J. K. Larsen. *Applied Mathematical Models in Human Physiology*, SIAM, Philadelphia (2004).

